KEPLER-4b: A HOT NEPTUNE-LIKE PLANET OF A G0 STAR NEAR MAIN-SEQUENCE TURNOFF[*]

William J. Borucki[1], David G. Koch[1], Timothy M. Brown[2], Gibor Basri[3], Natalie M. Batalha[4],
Douglas A. Caldwell[1], William D. Cochran[5], Edward W. Dunham[6], Thomas N. Gautier III[7], John C. Geary[8],
Ronald L. Gilliland[9], Steve B. Howell[10], Jon M. Jenkins[1,11], David W. Latham[8], Jack J. Lissauer[1],
Geoffrey W. Marcy[3], David Monet[12], Jason F. Rowe[1], and Dimitar Sasselov[8]

[1] NASA/Ames Research Center, Moffett Field, CA 94035, USA
[2] Las Cumbres Observatory Global Telescope, Goleta, CA 93117, USA
[3] University of California–Berkeley Astronomy Department, Berkeley, CA 94720, USA
[4] San Jose State University Department of Physics and Astronomy, San Jose, CA 95192, USA
[5] University of Texas at Austin Department of Astronomy, Austin, TX 78712, USA
[6] Lowell Observatory, Flagstaff, AZ 86001, USA
[7] Jet Propulsion Laboratory/California Institute of Technology, Pasadena, CA 91109, USA
[8] Harvard-Smithsonian Center for Astrophysics, Cambridge, MA 02138, USA
[9] Space Telescope Science Institute, Baltimore, MD 21218, USA
[10] National Optical Astronomy Observatories, Tucson, AZ 85726, USA
[11] SETI Institute, Mountain View, CA 94043, USA
[12] United States Naval Observatory, Flagstaff, AZ 86002, USA

ABSTRACT

Early time-series photometry from NASA's *Kepler* spacecraft has revealed a planet transiting the star we term Kepler-4, at R.A. $= 19^{\rm h}02^{\rm m}27\rlap{.}^{\rm s}68$, $\delta = +50°08'08\rlap{.}''7$. The planet has an orbital period of 3.213 days and shows transits with a relative depth of 0.87×10^{-3} and a duration of about 3.95 hr. Radial velocity (RV) measurements from the Keck High Resolution Echelle Spectrometer show a reflex Doppler signal of $9.3^{+1.1}_{-1.9}$ m s^{-1}, consistent with a low-eccentricity orbit with the phase expected from the transits. Various tests show no evidence for any companion star near enough to affect the light curve or the RVs for this system. From a transit-based estimate of the host star's mean density, combined with analysis of high-resolution spectra, we infer that the host star is near turnoff from the main sequence, with estimated mass and radius of $1.223^{+0.053}_{-0.091}$ $M_\odot$ and $1.487^{+0.071}_{-0.084}$ $R_\odot$. We estimate the planet mass and radius to be $\{M_{\rm P}, R_{\rm P}\} = \{24.5 \pm 3.8\ M_\oplus, 3.99 \pm 0.21\ R_\oplus\}$. The planet's density is near 1.9 g cm^{-3}; it is thus slightly denser and more massive than Neptune, but about the same size.

Key words: planetary systems – stars: fundamental parameters – stars: individual (Kepler-4, KIC 11853905, 2MASS 19022767+5008087)

1. INTRODUCTION

Transiting extrasolar planets provide unparalleled opportunities for detailed study of the physical characteristics of distant solar systems. Since the first transiting planet detection a decade ago, ground-based surveys such as TrES, HAT, and Super-WASP (Alonso et al. 2004; Bakos et al. 2004; Pollacco et al. 2006) and the space-borne telescope *CoRoT* (Baglin et al. 2007) have located more than 50 transiting planets, spanning a large range in size and mass. With the advent of NASA's *Kepler Mission*, we have a new and extraordinarily sensitive tool for studying transiting planets. *Kepler* has enough sensitivity to detect Earth-size planets orbiting in the habitable zones of Sun-like stars during its planned 3.5-year mission (Koch et al. 2010; Borucki et al. 2010). The first science data to return after *Kepler's* launch in 2009 March were time series from a 9.7 day commissioning run, followed after a 1.6 day gap by a 33.5 day science run. Here, we describe the transiting planet Kepler-4b, one of several transiting planets discovered during these first two observing intervals.

2. OBSERVATIONS, ANALYSIS, AND TESTS FOR FALSE POSITIVES

Observations of the *Kepler* target field commenced 2009 May 1; the data that we describe here are long cadence (LC) photometry, which correspond to integration times of 29.426 minutes. For a full description of the *Kepler* field of view, observing modes, and data processing pipeline, see Jenkins et al. (2010) and Caldwell et al. (2010). For *Kepler* target stars brighter than $r = 13$, the rms photometric precision attained for relative flux time series is typically better than 2×10^{-4} per 29 minutes integration (Gilliland et al. 2010). We detrended photometry from the mission data reduction pipeline and searched it for significant transit-like events using the procedures described by Jenkins et al. (2010) and by Batalha et al. (2010).

One of the transiting planet candidates identified by the process just described was the star that we now term Kepler-4. This star is uncommonly bright by *Kepler* standards. Its Kepler magnitude (AB magnitude averaged over the *Kepler* bandpass) is Kepmag $= 12.211$. Characteristics of this star are given in Table 1; briefly, it is a somewhat metal-rich ([Fe/H] $= +0.17 \pm 0.06$) star of nearly solar temperature (5857 ± 120 K), evidently seen near the end of its main-sequence lifetime, as explained below.

Table 1
System Parameters for Kepler-4

Parameter	Value	Notes
Transit and orbital parameters		
Orbital period P (d)	3.21346 ± 0.00022	A
Midtransit time E (HJD)	2454956.6127 ± 0.0015	A
Scaled semimajor axis $a/R_\star$	$6.47^{+0.26}_{-0.28}$	A
Scaled planet radius $R_P/R_\star$	$0.02470^{+0.00031}_{-0.00030}$	A
Impact parameter $b \equiv a \cos i / R_\star$	$0.022^{+0.234}_{-0.022}$	A
Orbital inclination i (deg)	$89.76^{+0.24}_{-2.05}$	A
Orbital semi-amplitude K (m s^{-1})	$9.3^{+1.1}_{-1.9}$	A, B
Orbital eccentricity e	0 (adopted)	A, B
Center-of-mass velocity γ (m s^{-1})	-1.27 ± 1.1	A, B
Observed stellar parameters		
Effective temperature $T_{\rm eff}$ (K)	5857 ± 120	C
Spectroscopic gravity $\log g$ (cgs)	4.25 ± 0.10	C
Metallicity [Fe/H]	$+0.17 \pm 0.06$	C
Projected rotation $v \sin i$ (km s^{-1})	2.2 ± 1.0	C
Mean radial velocity (km s^{-1})	-61.0 ± 0.10	B
Derived stellar parameters		
Mass $M_\star (M_\odot)$	$1.223^{+0.053}_{-0.091}$	C, D
Radius $R_\star (R_\odot)$	$1.487^{+0.071}_{-0.084}$	C, D
Surface gravity $\log g_\star$ (cgs)	4.17 ± 0.04	C, D
Luminosity $L_\star (L_\odot)$	$2.26^{+0.66}_{-0.48}$	C, D
Absolute V magnitude M_V (mag)	4.00 ± 0.28	D
Age (Gyr)	4.5 ± 1.5	C, D
Distance (pc)	550 ± 80	D
Planetary parameters		
Mass M_P (M_J)	0.077 ± 0.012	A, B, C, D
Radius R_P (R_J, equatorial)	0.357 ± 0.019	A, B, C, D
Density ρ_P (g cm^{-3})	$1.91^{+0.36}_{-0.47}$	A, B, C, D
Surface gravity $\log g_P$ (cgs)	$3.16^{+0.06}_{-0.10}$	A, B, C, D
Orbital semimajor axis a (AU)	0.0456 ± 0.0009	E
Equilibrium temperature $T_{\rm eq}$ (K)	1650 ± 200	F

Notes. A: based primarily on the photometry. B: based on the RVs. C: based on spectrum analysis (FIES/MOOG or HIRES/SME). D: based on the Yale–Yonsei evolution tracks. E: based on Newton's version of Kepler's third law. F: assumes Bond albedo = 0.1 and complete redistribution.

Figure 1 shows the light curve for Kepler-4, folded with a period of 3.21346 days.[13] Since the transit signal was clear, we proceeded with follow-up observations as described in Gautier et al. (2010) and Batalha et al. (2010). Experience with both ground- and space-based transit observations shows that a fairly large fraction of events that resemble planetary transits are actually caused by eclipses involving only stars, or eclipses with properties that are significantly confused by diluting light from one or more stellar companions, either physical or projected. For this reason, we designed our follow-up observations to determine whether the light-curve dips can be ascribed to a transiting planet; if not, what eclipsing star or other process might be responsible for them; and if so, what the properties of the host star and its planet might be.

Ground-based visible-light speckle imaging from the WIYN Telescope, NIR adaptive-optics imaging from the Mt. Palomar 5 m telescope, and also with the NIRC2 camera on the Keck
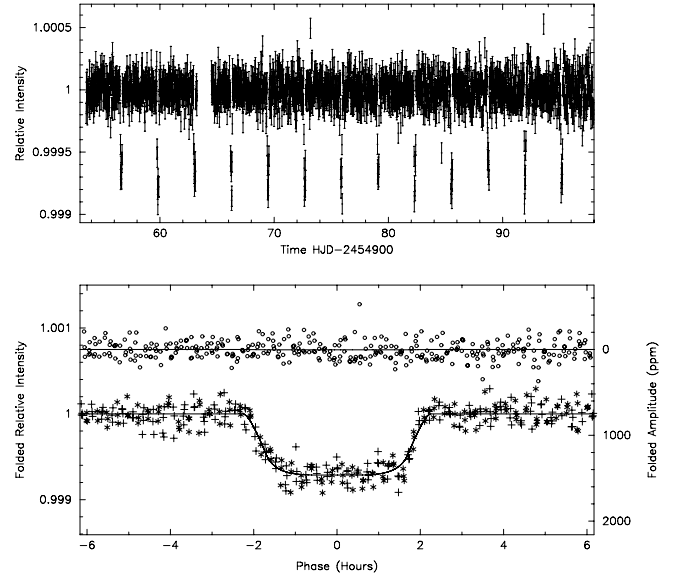
Figure 1. Phased light curve of Kepler-4b containing 13 transits observed by the *Kepler* photometer between 2009 May 1 and 2009 June 15. The upper panel shows the full 44 day time series after detrending. The bottom panel shows the light curve folded with the orbital period; different plot symbols denote odd- and even-numbered transits. The lower curve shows transit data overplotted on the fitted transit model. The upper curve covers the expected time of occultation, with the fitted (essentially constant) model overplotted. This model assumes a circular orbit. The full folded light curve (not shown here) gives no evidence for an occultation at any phase. For transit and orbital parameters, see Table 1.

telescope all show Kepler-4 as an isolated star, apart from a neighbor that is 3.5 mag fainter at a distance of 11″9. We estimate that this star contributes 2% ± 2% to the flux we measure for Kepler-4, which dilutes the transit by a factor of 1.02 ± 0.02. We take this dilution and its uncertainty into account in computing the planetary radius R_P and its probable errors. Limits on nearby companions are described by Batalha et al. (2010); the imagery rules out background eclipsing binaries that might simulate the observed transits, up to a magnitude difference of 9.8 in the H band, for companions between 0″12 and 3″0 from Kepler-4. We have also searched for motion of the image centroid that is correlated with the transits, finding no such motion with a limit of 4×10^{-4} arcsec.

Two reconnaissance spectra obtained with the TRES spectrograph on the 1.5 m Tillinghast Reflector at the Whipple Observatory showed a velocity variation of less than 150 m s^{-1} over 5 days. Accordingly, we obtained RV measurements with the High Resolution Echelle Spectrometer (HIRES) on the Keck I telescope (Vogt et al. 1994). Figure 2 shows the RV data for Kepler-4, folded with the transit period and shifted so that transit center occurs at zero phase. Assuming zero eccentricity, we obtained a RV variation with phase that is consistent with the observed light curve, with a reflex velocity amplitude K of $9.3^{+1.1}_{-1.9}$ m s^{-1} and velocity residuals of only 3.6 m s^{-1}. We also performed a fit in which we allowed the eccentricity e to float. This gave $e = 0.22 \pm 0.08$ and $K = 10.0$ m s^{-1}; the reduced χ^2 improved only slightly. Finally, a Monte Carlo bootstrap (described below) that simultaneously fits all photometry and RV values, and that is consistent with stellar evolution models, gives $e \sin \omega = -0.003 \pm 0.058$ and $e \cos \omega = -0.005 \pm 0.057$. There is thus only marginal evidence for a noncircular orbit. In the analysis below, we do however account throughout for the possible range of e and ω in our estimates of stellar and planetary parameters and their uncertainties. Given the integration
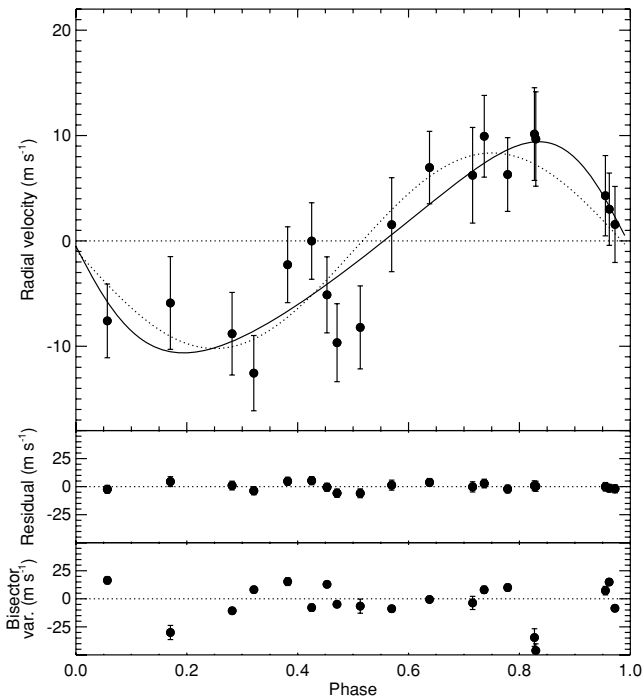
Figure 2. Top panel: the phased RV curve of Kepler-4, consisting of 19 epochs observed using the Keck/HIRES, spanning 69 days. The dashed overplotted curve is a fit assuming a circular orbit, phased to match the transit photometry. The solid curve shows the best-fit eccentric orbit, with $e = 0.22$. Middle panel: O–C residuals of velocities relative to the circular orbit fit. Bottom panel: bisector span for each epoch, measured between the 40% and 90% depth points in the cross-correlation against a representative spectrum.

3. PROPERTIES OF THE PLANET AND HOST STAR

3.1. Method for Estimating Host Star Masses and Radii

The *Kepler* photometer produces a light curve that implies the planetary radius in units of the host star radius. Likewise, ground-based follow-up Doppler spectroscopy yields the mass of the planet in terms of the host star's mass. Thus, having accurate values for the host star's fundamental parameters—mass, radius, effective temperature, and composition—will be essential for carrying out *Kepler's* mission to characterize planets circling distant stars.

But it is also possible to reverse this logical flow, and use transiting planets as probes of their host stars. Seager & Mallén-Ornelas (2003) derived expressions relating the light curve to the mean density ρ_* of a transiting planet's host star. They showed that ρ_* can be expressed in terms of the planet's orbital period, the fractional flux obstructed by the planet, and two different measures of the transit duration. All of these quantities are directly measurable from the light curve, and their interpretation depends only on Newtonian mechanics and geometry.

The method we use (henceforth, the ρ_* method) for estimating stellar radii and other parameters is an implementation of that described by Sozzetti et al. (2007) and subsequently used by, e.g., Bakos et al. (2007), Winn et al. (2007), and Charbonneau et al. (2007). This technique has become the most trusted way of obtaining information about transiting planets' host stars, as illustrated by Torres et al. (2008).

The basis for the ρ_* method is that, although stellar models are ordinarily taken to depend on five parameters (mass, age, metallicity, initial helium abundance, and mixing length) $= \{M_*, A_*, [Z], Y_0, \alpha\}$, the last two of these do not vary much among stars, and for practical purposes are often taken as known. In particular, the much-used Yonsei–Yale (henceforth YY) model grid (Yi et al. 2001) uses specified values for the mixing length and for the initial helium abundance. In this approximation, stars are described by a three-dimensional grid of models, parameterized by mass, age, and metallicity. Every transiting planet discovered by *Kepler* and followed up with reconnaissance spectroscopy has an observed transit light curve that constrains ρ_*, and also spectrographic estimates of T_{eff} and $[Z]$. Moreover, for main-sequence stars, the problem of inferring stellar structure parameters from the three observables $\{\rho_*, T_{\mathrm{eff}}, [Z]\}$ is usually well posed, allowing precise conclusions without important degeneracies. Thus, the quantities that we may readily observe usually suffice to isolate a single set of model parameters (mass, age, metallicity); from these, we may compute any other global property (e.g., radius, luminosity, or surface gravity).

We implement the ρ_* method by searching a precomputed grid of models (interpolated from the YY models) to find the one that best matches the observations in a χ^2 sense. The optimization problem involves interpolating within the given model grid and performing a conventional (e.g., "amoeba") hill-climbing optimization search. Estimating errors and verifying that the search has converged to the global optimum is done using a Markov chain Monte Carlo (MCMC) process. To allow for possible systematic errors in the spectrographic analysis, we took uncertainties in $[Z]$ to be the larger of 0.06 dex and the quoted value, and twice the quoted value for T_{eff}. For ρ_*, we used a parameterization of the (often highly asymmetric) error distribution estimated from a jackknife analysis of the photometry. Not all parameter choices $\{M_\star, A_*, [Z]\}$ permitted by a given ρ_* are consistent with the photometry, and vice versa.
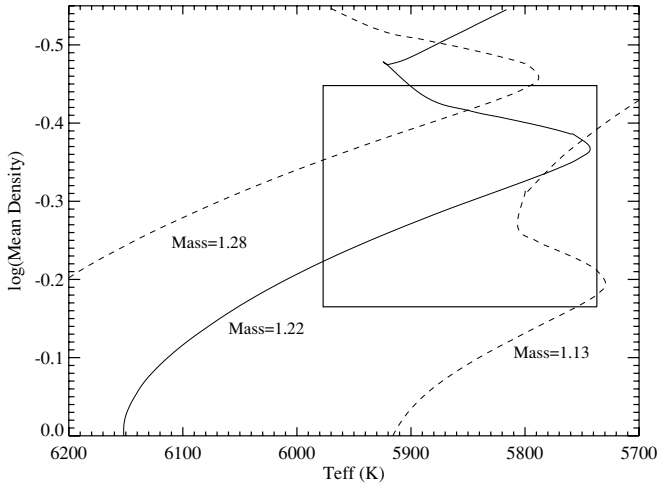
times of the spectra and Kepler-4's brightness, T_{eff}, and slow rotation ($v \sin i = 2.2 \pm 1.0$ km s^{-1}), the residuals are consistent with expectations. We also used the HIRES spectra to search for variations in the shapes of line bisectors; the component of the bisector span that is in phase with the orbital period has amplitude -1.2 ± 4.2 m s^{-1} (with uncertainty estimated from the bisector scatter), offering no support for the presence of a blended eclipsing binary star.

We can reject many photometric blend scenarios, but not all. Kepler-4b's long transit duration rules out hierarchical triple systems in which the primary of the eclipsing pair contributes less than about 25% of the system luminosity. Near-twin star systems permitted by this constraint would lead to errors in the planet radius and mass by factors of a few—these would be serious, but not large enough that transits by stars could be confused with those by planets. Moreover, virtually all transiting planet parameter estimates are vulnerable to confusion of this sort. An unresolved background eclipsing binary star might accurately simulate the transit light curve, but such a system would not likely produce the very small observed RV variation, nor the small line bisector variation. The most plausible remaining blend scenario involves an unresolved background transiting Jupiter-size planet. Such a blend could be consistent with all current observations, though the required coincidence in apparent position is very unlikely a priori.

Thus, although some kinds of confusing photometric blends are possible, there is no evidence for them. In what follows, we assume that the observed light curve results from transits by a rather small extrasolar planet across the face of a normal, single, Sun-like star.

Figure 3. Yonsei–Yale evolutionary tracks for stars with $[Z] = 0.17$ and masses between 1.13 and 1.28 $M_\odot$, plotted in the ρ_*–$T_{\rm eff}$ plane. The box indicates our adopted observational constraints on ρ_* and $T_{\rm eff}$. For this range of masses, all tracks lie partly inside the error box, showing that multiple solutions are possible that satisfy these constraints.

Moreover, in the light-curve analysis, the estimated ρ_* depends somewhat on the initial guess for $M_\star$ (Koch et al. 2010) and on the range of orbital eccentricity allowed by the observations. To account for the different information supplied by these two kinds of model fitting, we iterated the solution by putting the MCMC probability distributions back into the light-curve analysis. The most likely parameter values and uncertainty distributions we report below are the result of this once-iterated fit.

Brown (2010) has tested the ρ_* method against a sample of 169 stars (mostly members of eclipsing binaries taken from the compilation by Torres et al. 2009) that have accurately known masses and radii. This comparison shows that method's systematic errors do not exceed 2%–3% in radius, and about 6%–9% in mass. Random errors appear to arise about equally from uncertainties in the estimated stellar $T_{\rm eff}$ and metallicity, and from uncertainties in the masses and radii inferred for the eclipsing binary components using traditional (but largely model-independent) techniques. Systematic errors arise mostly because rapidly rotating and hence magnetically active stars are seen to have larger radii than slowly rotating stars with otherwise similar properties (e.g., Torres et al. 2006; López-Morales 2007; Morales et al. 2008). The sample of eclipsing binary stars consists almost entirely of such fast rotators; this causes an excess of up to several percent in the actual radii of stars of sub-solar mass, relative to the YY models. On the other hand, the host stars of confirmed transiting planets found by *Kepler* are mostly slow rotators (if only because it is difficult to measure precise RVs of rapidly rotating stars). Errors in these estimates should therefore be dominated by measurement errors, especially in $[Z]$ and in ρ_*.

3.2. The Star Kepler-4

Simultaneous fits to the transits of Kepler-4b and to the RV data (allowing nonzero eccentricity) yield the ratio of orbital semimajor axis a to stellar radius $R_\star$, namely $a/R_\star = 6.47^{+0.26}_{-0.28}$, which with the orbital period gives $\rho_* = 0.50 \pm 0.16$ g cm^{-3}. This is a low value, roughly 1/3 that of the Sun, suggesting that Kepler-4 must have evolved considerably away from the zero-age main sequence. Applying the ρ_* method confirms this conclusion, and in fact finds a range of model parameters, all of

which fit the observations almost equally well, but which imply distinct evolutionary states for the star. Figure 3 shows evolution tracks for three models having masses between 1.13 $M_\odot$ and 1.28 $M_\odot$. In this mass range, old main-sequence stars have small convective cores. Because of efficient mixing, these cores suffer hydrogen exhaustion all at once, following which the entire star must compress and heat until the central temperature rises enough to start shell hydrogen burning. The blue-going hook at main-sequence turnoff is a result of this compression. In the case of Kepler-4, the observed ρ_* and $T_{\rm eff}$ (indicated by the error box in Figure 3) are closely matched by each of the evolution tracks, albeit at different ages and with models occupying different evolutionary states. Thus, for the lowest-mass star to fit the observations, it must have just finished its core-contraction phase, and be on its way to becoming a shell-burning subgiant. The highest-mass star to fit the same observations must still be on the main sequence but nearing hydrogen exhaustion in its core, just poised to begin core contraction.

It is not possible to distinguish among these possibilities using existing observations. Although the masses of acceptable models differ by as much as 13%, the radii differ by only 1/3 as much (in order to give the same observed mean density). This radius difference would cause a difference in $\log(g)$ that is too small to measure with current methods. Likewise, the luminosity difference of about 8% implies a parallax difference of only 4%, also too small to discern at this star's likely distance of about 550 ± 80 pc. Asteroseismology may however offer a way out of this quandary. Because of the star's relatively large luminosity and apparent brightness, it may be possible to measure the frequencies of its pulsation modes, and hence distinguish among the feasible evolution scenarios. Kepler-4 is now being observed with *Kepler's* short (60 s) cadence; the mission will report pulsation properties estimated from these data if and when the pulsation signals rise above the noise.

We list the inferred properties of Kepler-4 in Table 1. For the quantities $M_\star$ and $R_\star$ we give uncertainties that include the effects of observational uncertainties, of uncertainty in orbital eccentricity, and of uncertainty in the host star's evolutionary state.

3.3. The Planet Kepler-4b

Given the properties of its host star, the depth of transits due to Kepler-4b implies a planetary radius of 0.357 ± 0.019 $R_{\rm J} = 3.99 \pm 0.21$ $R_\oplus$, and a mass of 0.077 ± 0.012 $M_{\rm J} = 24.5 \pm 3.8$ $M_\oplus$. As with $M_\star$ and $R_\star$, these values and uncertainties should be interpreted as describing the centers and 68% probability points of the marginal probability distributions, accounting for all of the uncertainties. Kepler-4b is therefore slightly more massive than Neptune, and about the same size. Its mean density is about 1.9 g cm^{-3}, greater than that of Jupiter and considerably larger than that of Saturn. Assuming a 10% Bond albedo and efficient heat redistribution to the planet's night side, its equilibrium temperature is 1650 ± 200 K (Koch et al. 2010). Radial velocity data provide no evidence for other massive planets in small orbits. Because of the limited time span and precision of the extant RV observations, it is however impossible to rule out such planetary companions.

4. DISCUSSION

Figure 4 shows Kepler-4 in a mass–radius diagram that spans the range so far occupied by small transiting exoplanets. Kepler-4b is the third known transiting Neptune-like planet,
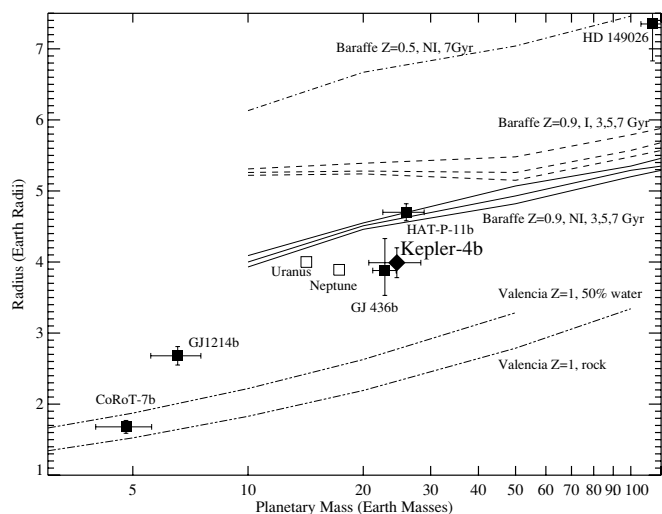
Figure 4. Kepler-4b is shown in a mass–radius plot, along with other hot Neptunes, the hot super-Earths CoRoT-7b (Léger et al. 2009; Queloz et al. 2009) and GJ1214b (Charbonneau et al. 2009), and model curves by Baraffe et al. (2008) and by Valencia et al. (2007), showing increasing heavy-element fractions toward the bottom of the figure. Multiple dashed and solid curves show model results for differing ages; "I" indicates irradiated and "NI" non-irradiated models. Kepler-4b appears to be denser than HAT-P-11b but similar to GJ436b, denser than the non-irradiated $Z = 0.9$ model by Baraffe et al. (2008), but much less dense than is expected for a water or rocky planet.

together with GJ436b (Gillon et al. 2007) and HAT-P-11b (Bakos et al. 2010); all three have masses and radii equal to or larger than those of Neptune and Uranus. The most important differences between the three exoplanets are their host stars and the incident flux the planets receive (GJ436b: M dwarf, T_{eq} = 650 K; HAT-P-11b: K dwarf, 880 K; Kepler-4b: G subgiant, 1650 K). On the mass–radius diagram Kepler-4b and GJ436b both lie below the $Z = 0.9$ Baraffe et al. (2008) non-irradiated model. In these models, $Z = 0.9$ denotes that the planet has a 10% by mass envelope of H and He, and "non-irradiated" corresponds roughly to the case of GJ436b and cooler. The fact that Kepler-4b and GJ436b have essentially identical radii (3.88 ± 0.15 $R_\oplus$ for GJ436b from NASA EPOXI (Ballard et al. 2009) as compared to 3.99 ± 0.21 $R_\oplus$ for Kepler-4) at the same mass, despite Kepler-4b's high T_{eq}, implies a difference in bulk composition. We suggest that Kepler-4b has an H/He envelope of about 4%–6% by mass and a correspondingly higher water and rock fraction. However, the inherent degeneracy in this part of the mass–radius diagram means that the H/He envelope might be slightly more massive if the rock-to-water ratio in the interior of Kepler 4b is unusually high (i.e., significantly higher than in Neptune or Uranus). Nevertheless, we can state with a measure of confidence that there are no possible interior models for Kepler-4b with no H/He envelope and neither it nor GJ436b is compact enough to be a water-rich super-Earth.

The slightly eccentric orbits of the two previously known transiting Neptune-like planets, in similar potentials and at similar ages, suggest that their interiors are somewhat less dissipative to stellar tides than the giants in our solar system. Therefore, it would be very interesting to resolve whether the orbit of Kepler-4b has comparable eccentricity or is circular; the current observations are still inconclusive.

REFERENCES

Alonso, R., et al. 2004, ApJ, 613, L153
Baglin, A., Auvergne, M., Barge, P., Michel, E., Catala, C., Deleuil, M., & Weiss, W. 2007, in AIP Conf. 895, Fifty Years of Romanian Astrophysics, ed. C. Dumitrache, et al. (Melville, NY: AIP), 201
Bakos, G., Noyes, R. W., Kovács, G., Stanek, K. Z., Sasselov, D. D., & Domsa, I. 2004, PASP, 116, 266
Bakos, G. Á., et al. 2007, ApJ, 670, 826
Bakos, G. Á., et al. 2010, ApJ, 710, 1724
Ballard, S., et al. 2009, ApJ, submitted (arXiv:0909.2875)
Baraffe, I., Chabrier, G., & Barman, T. 2008, A&A, 482, 315
Batalha, N., et al. 2010, ApJ, 713, L103
Borucki, W.J., et al. 2010, Science, in press
Brown, T. M. 2010, ApJ, 709, 535
Caldwell, D., et al. 2010, ApJ, 713, L92
Charbonneau, D., Winn, J. N., Everett, M. E., Latham, D. W., Holman, M. J., Esquerdo, G. A., & O'Donovan, F. T. 2007, ApJ, 658, 1322
Charbonneau, D., et al. 2009, Nature, 462, 891
Gautier, T.N., et al. 2010, ApJ, submitted
Gilliland, R. L., et al. 2010, PASP, in press (arXiv:1001.0142v1)
Gillon, M., et al. 2007, A&A, 472, L13
Jenkins, J., et al. 2010, ApJ, 713, L87
Koch, D. G., et al. 2010, ApJ, 713, L79
Léger, A., et al. 2009, A&A, 506, 287
López-Morales, M. 2007, ApJ, 660, 732
Morales, J. C., Ribas, I., & Jordi, C. 2008, A&A, 478, 507
Pollacco, D. L., et al. 2006, PASP, 118, 1407
Queloz, D., et al. 2009, A&A, 506, 303
Seager, S., & Mallén-Ornelas, G. 2003, ApJ, 585, 1038
Sozzetti, A., Torres, G., Charbonneau, D., Latham, D. W., Holman, M. J., Winn, J. N., Laird, J. B., & O'Donovan, F. T. 2007, ApJ, 664, 1190
Torres, G., Andersen, J., & Giménez, A. 2009, A&AR, 13
Torres, G., Lacy, C. H., Marschall, L. A., Sheets, H. A., & Mader, J. A. 2006, ApJ, 640, 1018
Torres, G., Winn, J. N., & Holman, M. J. 2008, ApJ, 677, 1324
Valencia, D., Sasselov, D., & O'Connell, R. 2007, ApJ, 665, 1413
Vogt, S. S., et al. 1994, Proc. SPIE, 2198, 362
Winn, J., et al. 2007, ApJ, 657, 1098
Yi, S., Demarque, P., Kim, Y.-C., Lee, Y.-W., Ree, C. H., Lejeune, T., & Barnes, S. 2001, ApJS, 136, 417